Intrazeolite topotaxy: sodium-23 double-rotation NMR study of transition-metal hexacarbonyls and oxides encapsulated in sodium zeolite Y. [Erratum to document cited in CA117(4):342...

ARTICLE *in* THE JOURNAL OF PHYSICAL CHEMISTRY · NOVEMBER 1992

Impact Factor: 2.78 · DOI: 10.1021/j100202a094

4 AUTHORS, INCLUDING:

Saim Özkar
Middle East Technical University
298 PUBLICATIONS **5,161** CITATIONS
SEE PROFILE

Heloise O Pastore
University of Campinas
140 PUBLICATIONS **1,401** CITATIONS
SEE PROFILE

Intrazeolite Topotaxy: ^{23}Na Double-Rotation NMR Study of Transition-Metal Hexacarbonyls and Oxides Encapsulated in Sodium Zeolite Y

Raz Jelinek,

Materials Sciences Division, Lawrence Berkeley Laboratory, and Department of Chemistry, University of California, Berkeley, California 94720

Saim Özkar,† and Geoffrey A. Ozin*

Advanced Zeolite Materials Research Group, Lash Miller Chemical Laboratories, University of Toronto, 80 St. George St., Toronto, Ontario, Canada M5S 1A1 *(Received: December 17, 1991; In Final Form: March 3, 1992)*

^{23}Na double-rotation NMR (DOR) provides details on site specific adsorption and anchoring interactions in intrazeolite hexacarbonylmetal(0) complexes, $m\{M(CO)_6\}$–$Na_{56}Y$, where M = Mo and W, and their molecular photooxidation products, $n\{MO_{3-x}\}$–$Na_{56}Y$, over the full composition range $0 < m \leq 16$, $0 < n \leq 32$ and $0 \leq x \leq 1$. The shifts, intensities, and line shapes of the ^{23}Na DOR resonances carry information on the environments of the extraframework Na^+ binding sites within the zeolite lattice, as well as structural aspects of the guest species.

Introduction

Zeolites are crystalline nanoporous materials that have numerous uses as catalysts, adsorbents, gas separators, and ion exchangers.[1] Recently, advanced materials aspects of zeolites have been the focus of increasing activity.[2] The discrete, molecular size dimensions of the cavities offer the possibility of fabricating organized assemblies of atomic, molecular, and cluster guests using the zeolite framework as a "template".

A recent example of an intrazeolite topotactic reaction is the photooxidation of hexacarbonylmetal(0) complexes with dioxygen.[3,4] The reaction is carried out entirely within the porous framework of $Na_{56}Y$ zeolite, yielding an array of encapsulated metal(VI) oxides, according to the following reaction stoichiometry:

$$m\{M(CO)_6\}\text{–}Na_{56}Y + 9/2nO_2 \xrightarrow{h\nu} m\{MO_3\}\text{–}Na_{56}Y + 6nCO_2 \quad (1)$$

where M = Mo, W, and $0 \leq m \leq 16$.

The above reaction is clean and quantitative and leads to molecular analogues of the bulk MoO_3 and WO_3 semiconductor phases. An especially noteworthy feature of these intrazeolite metal oxides, is the ability to control their oxygen stoichiometries through vacuum thermal reductive–elimination of O_2, according to the following reactions:

$$n\{WO_3\}\text{–}Na_{56}Y \xrightarrow{300\ ^\circ C} n\{WO_{2.5}\}\text{–}Na_{56}Y \xrightarrow{400\ ^\circ C} n\{WO_2\}\text{–}Na_{56}Y \quad (2)$$

$$n\{MoO_3\}\text{–}Na_{56}Y \xrightarrow{400\ ^\circ C} n\{MoO_2\}\text{–}Na_{56}Y \quad (3)$$

These processes can be quantitatively reversed by exposing the reduced samples to O_2 gas at 400 and 300 °C, respectively.

Various analytical techniques, including diffraction, spectroscopy, and microscopy have been employed to elucidate structural and adsorption properties of zeolites and molecular sieves.[5] Solid-state NMR investigations have concentrated on probing the environments of silicon and aluminum which comprise the zeolite framework[6] or adsorbed species within the zeolite cavities such as ^{129}Xe.[7] Extraframework, charge-balancing Na^+ cations have an important role in determining the adsorption and catalytic properties of zeolites and might offer a more direct NMR probe of the zeolite inner surface. ^{23}Na nuclei, however, exhibit usually large quadrupolar broadening even upon magic angle spinning (MAS) which renders the interpretation of the NMR data quite difficult. The newly developed double-rotation (DOR) technique removes the anisotropic broadening of quadrupolar nuclei, thus facilitates a significantly better spectral resolution.[8]

Recently, we obtained high-resolution ^{23}Na DOR spectra of $Na_{56}Y$,[9] identifying specific Na^+ sites within the zeolite framework. In this work we extend the application of ^{23}Na DOR in order to detect and understand "guest-host" interactions within the sodium zeolite Y lattice. Analysis of the position, shape, and intensity of the ^{23}Na NMR resonances yields information on the environments of anchoring Na^+ sites. We discuss cooperative and symmetry effects at the extraframework Na^+ sites and structural aspects of the guest species, as they appear in the ^{23}Na DOR results.

Experimental Section

The various $n\{M(CO)_6\}$–$Na_{56}Y$ and $n\{MO_{3-x}\}$–$Na_{56}Y$ samples used in this study were synthesized according to procedures which are described elsewhere.[3,4] ^{23}Na DOR spectra were recorded in a 11.7-T magnetic field on a CMX-500 spectrometer using a home-built probe, whose features are described elsewhere.[10] Spinning speed was 5 kHz for the inner rotor and 600–800 Hz for the outer one. All samples were loaded into the inner rotor under rigorous anaerobic conditions. 1000–3000 acquisitions were accumulated in each experiment using 4-μs (30°) pulses, with 0.5-s delays. All spectra were zero-filled to 2 K data points, with application of 200-Hz Lorentzian broadening. The external reference was 0.1 M NaCl solution.

Results and Discussion

The $Na_{56}Y$ zeolite framework consists of AlO_4 and SiO_4 tetrahedra which form an interconnecting sodalite–cavity structure. The sodalite cage network produces a regular array of bigger α-cages (eight of these are contained in a unit cell), a schematic drawing of which is shown in Figure 1. Four distinct extraframework sites are located within the zeolite framework[1] as indicated in the figure: site I inside the hexagonal prism (located between two six-membered rings), site I′ within the sodalite cage (located above one six-ring), and two sites, II and III, inside the 13-Å α-cage (located above six- and four-rings, respectively).

A multiprong approach, including diffraction, spectroscopy, microscopy, thermal and chemical analyses, has been applied to all the aforementioned intrazeolite metal(0) hexacarbonyl precursors, $n\{M(CO)_6\}$–$Na_{56}Y$, and oxidation products, $n\{MO_{3-x}\}$–$Na_{56}Y$, in order to probe the structure, distribution, and properties of the encapsulated species. The proposed organization of the guests, for the special case of half-loading ($n = 16$) samples in $Na_{56}Y$, is illustrated schematically in Figures 2 and 3. In all cases, bond lengths and coordination numbers were estimated from Mo

†On leave from the Chemistry Department, Middle East Technical University, Ankara, Turkey, 06531.

*To whom correspondence should be addressed.

0022-3654/92/2096-5949$03.00/0

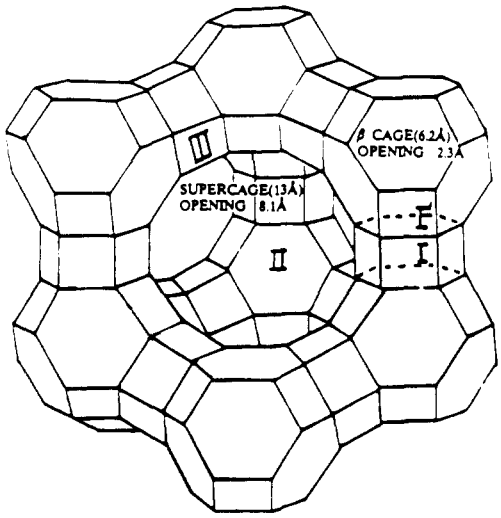

Figure 1. Schematic drawing of the $Na_{56}Y$ zeolite α-cage structure. Extraframework cation sites I, I', II, III are indicated.

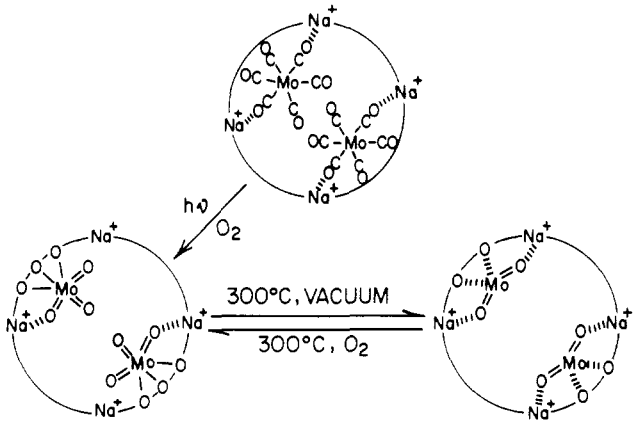

Figure 2. Schematic drawing of the intrazeolite structures and anchoring geometries of $16\{Mo(CO)_6\}$–$Na_{56}Y$, $16\{MoO_3\}$–$Na_{56}Y$, and $16\{MoO_2\}$–$Na_{56}Y$.[4,17]

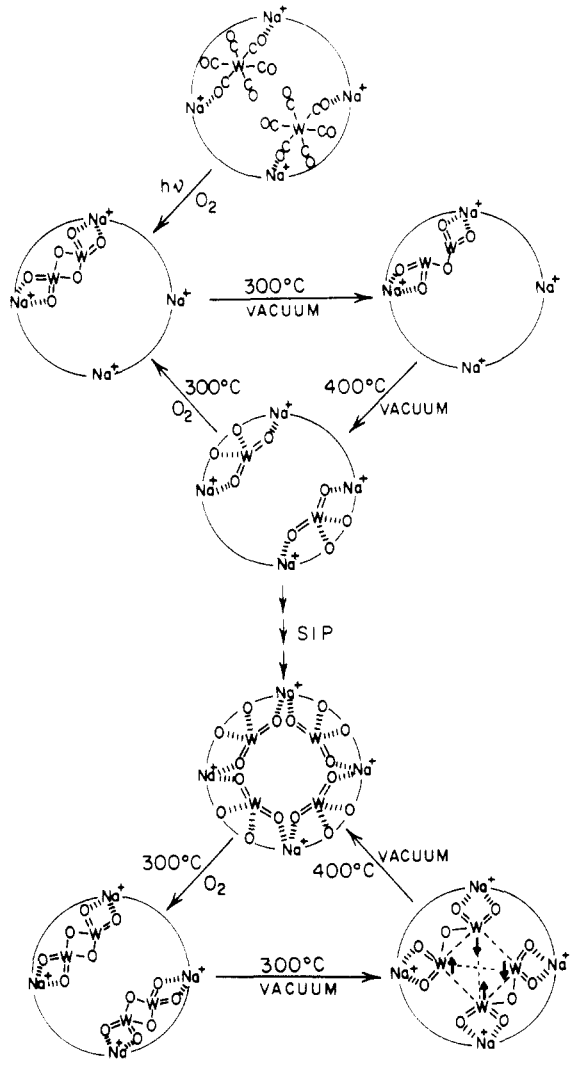

Figure 3. Schematic drawing of the intrazeolite structures and anchoring geometries of $16\{W(CO)_6\}$–$Na_{56}Y$, $16\{WO_3\}$–$Na_{56}Y$, $16\{WO_{2.5}\}$–$Na_{56}Y$, and $16\{WO_2\}$–$Na_{56}Y$.[11,12]

K-edge and W LIII-edge EXAFS structure analyses.[11,12] As shown in Figures 2 and 3, a ubiquitous feature for all intrazeolite $M(CO)_6$ precursors and MO_{3-x} products, is the proposed existence of anchoring interactions between the oxygen end of carbonyl ligands as well as the oxometal bonds, and the extraframework charge-balancing Na^+ cations located within the α-cages. The majority α-cage Na^+ cations under these circumstances[13] is seen to be a tetrahedral array of four site II Na^+ cations, each Na^+ being located above the center of an oxygen six-ring.

The existence of such $ZONa^+\cdots O$ interactions ($Z \equiv Si, Al$)[14a] has been deduced in earlier studies from a combination of site-specific frequency shifts in the Na^+ cation far-IR translatory modes, as well as line shifts and intensity alterations in the ^{23}Na MAS NMR spectra, induced by the introduction of $M(CO)_6$ and MO_{3-x} into the α-cages of the bare $Na_{56}Y$.[14b] In addition, Rb K-edge EXAFS structure analysis has been employed to evaluate $ZORb^+\cdots O$ anchoring interactions in some of these systems.[4] Taken together, the results of the above studies provide compelling evidence for the existence of anchoring interactions of the type illustrated in Figures 2 and 3. However, each method has particular interpretive difficulties that might render the conclusions not unequivocal. Specifically, the far-IR adsorption induced frequency shifts are usually only of the order of 2–5 cm^{-1} and might be blue or red shifted depending on the alterations in bonding and geometry around the Na^+ cation anchoring site.[14] The ^{23}Na MAS spectra of $Na_{56}Y$ and its guest-loaded derivatives were a convolution of poorly resolved quadrupolar-broadened resonances from the various Na^+ sites. The EXAFS derived adsorption induced changes in the Rb-O coordination numbers are the same order of magnitude as the experimental precision (20%). The ^{23}Na DOR results in Figures 4–9 provide a sensitive and direct probe of $ZONa^+\cdots O$ anchoring interactions in the α-cages, to more completely define the structure and properties of $M(CO)_6$ and MO_{3-x} guests in zeolite Y.

Intrazeolite Oxidation of $Mo(CO)_6$. Figure 4 shows the ^{23}Na DOR spectra of $n\{Mo(CO)_6\}$–$Na_{56}Y$ ($n = 0, 4, 8, 16$). The loading dependence is apparent in the NMR spectra as a substantial enhancement of the intensity of the ^{23}Na resonance at around −25 ppm. This peak is therefore ascribed to the anchoring Na^+ in site II within the α-cage, an assignment which was independently confirmed by a ^{23}Na DOR study of cation exchange in sodium zeolite Y.[9] The intensity of the signals at −5 and −41 ppm, ascribed to site I and I', respectively,[9] do not seem to be much affected by the $Mo(CO)_6$ adsorption. From inspecting Figure 4, one essentially "discovers" site II Na^+ signal through its selective anchoring to $Mo(CO)_6$ moieties (and other guest species, as will be discussed below). XRD and ND measurements[13,15] have established that approximately 55% of the extraframework Na^+ cations in dehydrated $Na_{56}Y$ are located inside the α-cage at site II, around 30% in the sodalite cage at site I', 7–8% in side I and the remainder at site III or unlocated. The ^{23}Na DOR spectrum of the bare $Na_{56}Y$, Figure 4a, features a different intensity ratio, in particular the relatively low intensity of the ^{23}Na peak at −29 ppm, which is ascribed to Na^+ cations in site II.

The relatively small peak assigned to site II Na^+, as well as the broad background signal around −30 ppm (Figure 4a) is probably due to a large distribution of chemical environments of Na^+ at this site. The spectral broadening might be brought about through motion, on the time scale of the NMR experiment, of

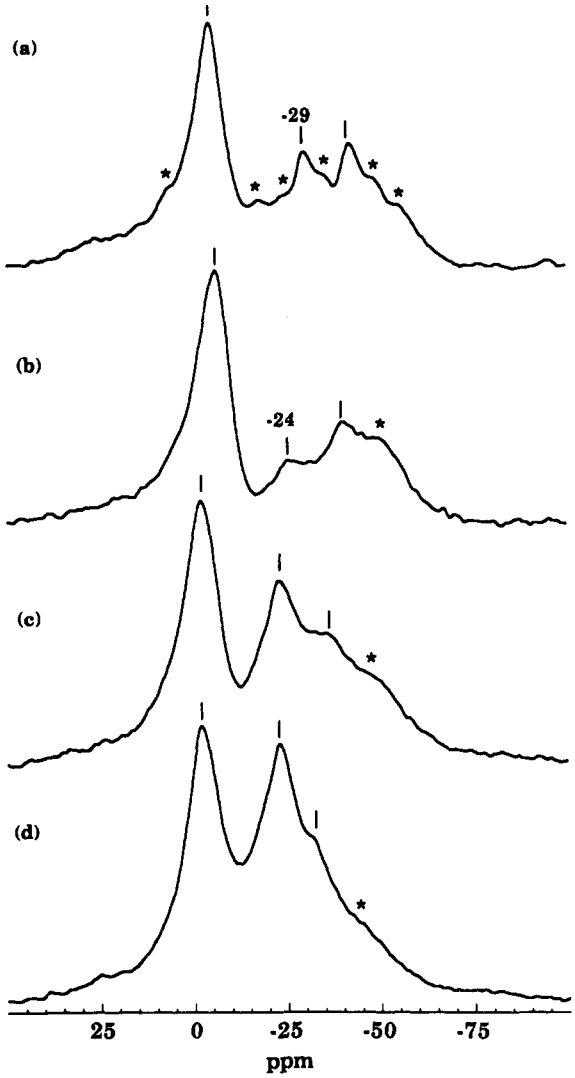

Figure 4. ^{23}Na DOR spectra of (a) dehydrated $Na_{56}Y$ and $Na_{56}Y$ loaded with (b) $4Mo(CO)_6$ guest molecules/unit cell, (c) $8Mo(CO)_6$ guest molecules/unit cell, (d) $16Mo(CO)_6$ guest molecules/unit cell. Asterisks denote spinning sidebands.

the site II Na^+ cations between accessible sites in the spacious α-cages. An additional contribution to the signal distribution could be the relatively large charge asymmetry at this Na^+ environment. In this sense, the transformation of "half-naked" $ZONa^+$ into coordinated $ZONa^+\cdots OC$, increases the symmetry around the site II Na^+ nucleus and/or reduces the Na^+ motion within the α-cage to the extent that the "missing" ^{23}Na intensity is recovered. Thus, the sharp signal ascribed to the site II Na^+, increases progressively as more $Mo(CO)_6$ guests are adsorbed within the zeolite framework, as shown in Figure 4b–d. A related effect has been observed in the ^{23}Na DOR spectra of a sodalite structure, containing Na_3^{3+} cluster guests in the β-cages.[16] In this material, a distinct ^{23}Na signal from the Na_3^{3+} clusters is observed in the hydrated sample but is broadened considerably, essentially "disappearing", upon removal of the water molecules.

The ^{23}Na DOR spectra of the oxidized $16\{Mo(CO)_6\}$–$Na_{56}Y$ species, reactions 1 and 3 are shown in Figure 5. The NMR results of both the photooxidized product, $16\{MoO_3\}$–$Na_{56}Y$, Figure 5c, and the further thermally reduced guest, $16\{MoO_2\}$–$Na_{56}Y$, Figure 5d, feature signals due to Na^+ in site II, although with significantly different intensities between the materials. MoO_3 is a monomer, considered to exhibit a trigonal pyramidal structure, and anchored to three framework oxygens through the metal vertice,[17] as illustrated in Figure 2. The disposition of the oxometal bonds in the trigonal pyramid is such that only a single oxygen end can essentially interact with an adjacent site II Na^+ cation. Therefore, whereas two $Mo(CO)_6$ are anchored to *four*

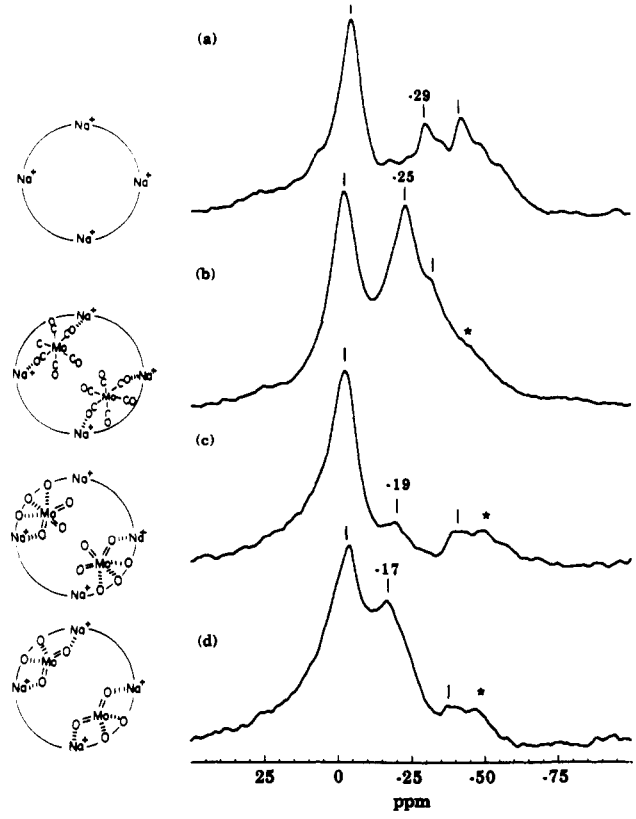

Figure 5. ^{23}Na DOR spectra of (a) dehydrated $Na_{56}Y$, (b) $16\{Mo(CO)_6\}$–$Na_{56}Y$, and oxidation products (c) $16\{MoO_3\}$–$Na_{56}Y$; (d) $16\{MoO_2\}$–$Na_{56}Y$. Asterisks denote spinning sidebands.

site II Na^+ in the α-cage, as shown in Figure 2, only *two* site II Na^+ cations will interact with the two $2MoO_3$ photooxidation products. Indeed, the ^{23}Na DOR spectrum of $16\{MoO_3\}$–$Na_{56}Y$, Figure 5c, shows a substantially reduced site II peak intensity, as essentially only *half* of the anchored Na^+ cations in the precursor sample, Figure 5b, are still bound in the photooxidized product.

Following the thermal reductive elimination of O_2, reaction 3, encapsulated MoO_2 molecular guests are produced inside the α-cages as illustrated in Figure 2. MoO_2 molecules have, in a similar way as the $Mo(CO)_6$ complexes, geometries that facilitate anchoring interactions to *two* site II Na^+ cations. Accordingly, the intensity of the signal at −19 ppm in $16\{MoO_2\}$–$Na_{56}Y$, Figure 5d, increases significantly compared to the respective Na^+ site II peak of $16\{MoO_3\}$–$Na_{56}Y$, Figure 5c. Incidentally, we observe a shift in the ^{23}Na resonance peak ascribed to site II, from −25 ppm in $16\{Mo(CO)_6\}$–$Na_{56}Y$, Figure 5b, to around −18 ppm in the MoO_3 and MoO_2 loaded samples, Figure 5c,d, respectively. This shift might indicate a different electronic interaction between the extraframework Na^+ and oxygen end of the carbonyl and oxomolybdenum bond, respectively.

Intrazeolite Oxidation of $W(CO)_6$. Figures 6–9 feature the ^{23}Na DOR spectra of the intrazeolite tungsten hexacarbonyl and oxide series, Figure 3 and reactions 1 and 2. The DOR spectrum of $16\{W(CO)_6\}$–$Na_{56}Y$, Figure 6b, is almost identical to the respective molybdenum precursor, $16\{Mo(CO)_6\}$–$Na_{56}Y$, shown in Figure 5b. The similarity of the NMR spectra indicates that the anchoring interactions and guest arrangements in both tungsten and molybdenum precursor materials are probably identical.

Photooxidation of the parent material $16\{W(CO)_6\}$–$Na_{56}Y$ produces $16\{WO_3\}$–$Na_{56}Y$, reaction 1, which is best viewed as a supralattice of W_2O_6 dimers (W^{6+}/W^{6+}) within the zeolite framework.[11,12] As shown in Figure 3, this configuration produces anchoring interactions of the W_2O_6 dimer with *two* site II Na^+ cations, through the oxygen end of the terminal oxotungsten bonds of the molecule. Accordingly, we observe a significant decrease in the ^{23}Na resonance ascribed to site II in the spectrum of the photooxidation product, Figure 6c, since *twice as many* Na^+

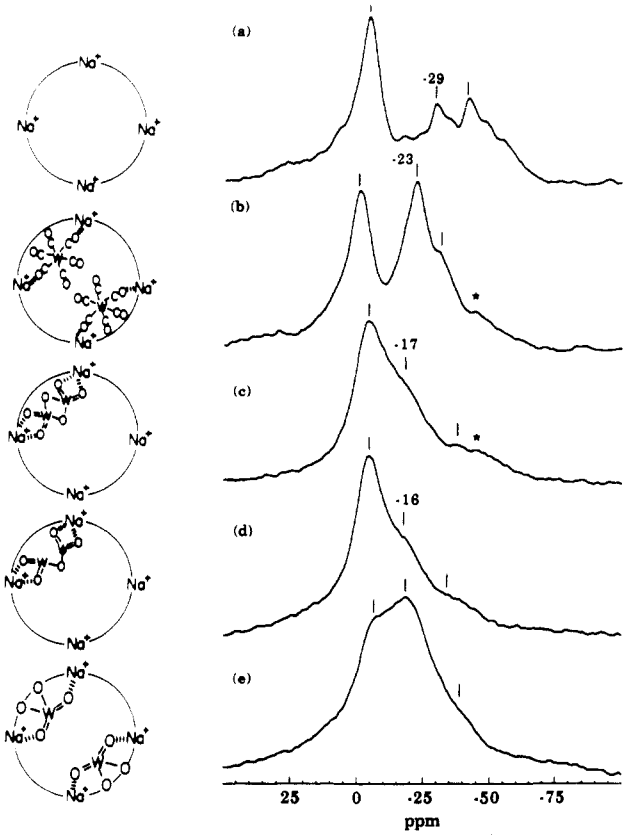

Figure 6. ^{23}Na DOR spectra of (a) dehydrated $Na_{56}Y$, (b) $16\{W(CO)_6\}$–$Na_{56}Y$, and oxidation products (c) $16\{WO_3\}$–$Na_{56}Y$, (d) $16\{WO_{2.5}\}$–$Na_{56}Y$, and (e) $16\{WO_2\}$–$Na_{56}Y$. Asterisks denote spinning sidebands.

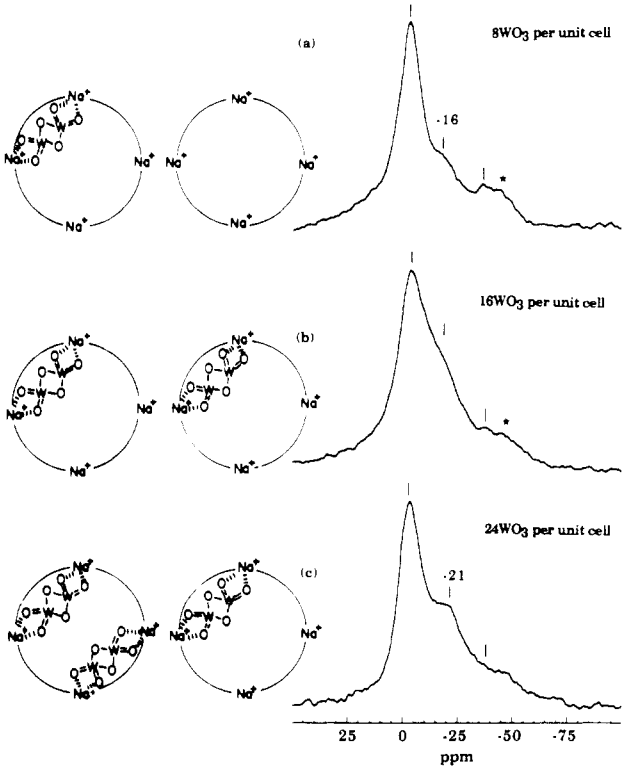

Figure 7. ^{23}Na–DOR spectra of (a) $8\{WO_3\}$–$Na_{56}Y$, (b) $16\{WO_3\}$–$Na_{56}Y$, and (c) $24\{WO_3\}$–$Na_{56}Y$. A schematic illustration of the structural arrangement of the guest species in two adjacent α-cages is shown on the left on each spectrum. Asterisks denote spinning sidebands.

cations were anchored in the parent precursor material, $16\{W(CO)_6\}$–$Na_{56}Y$, see Figure 3. The signal due to site II Na^+ in $16\{WO_3\}$–$Na_{56}Y$, Figure 6c, appears as a shoulder, at around −17

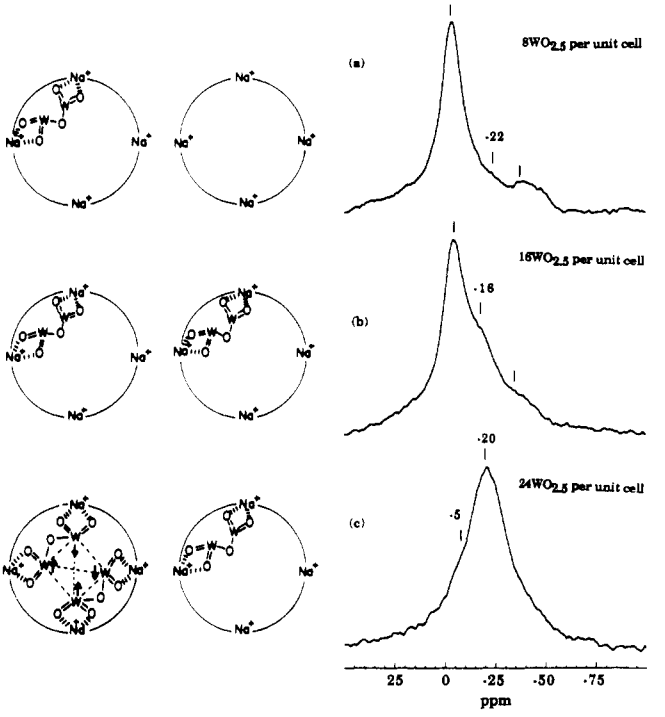

Figure 8. ^{23}Na–DOR spectra of (a) $8\{WO_{2.5}\}$–$Na_{56}Y$, (b) $16\{WO_{2.5}\}$–$Na_{56}Y$, and (c) $24\{WO_{2.5}\}$–$Na_{56}Y$. A schematic illustration of the structural arrangement of the guest species in two adjacent α-cages is shown on the left on each spectrum.

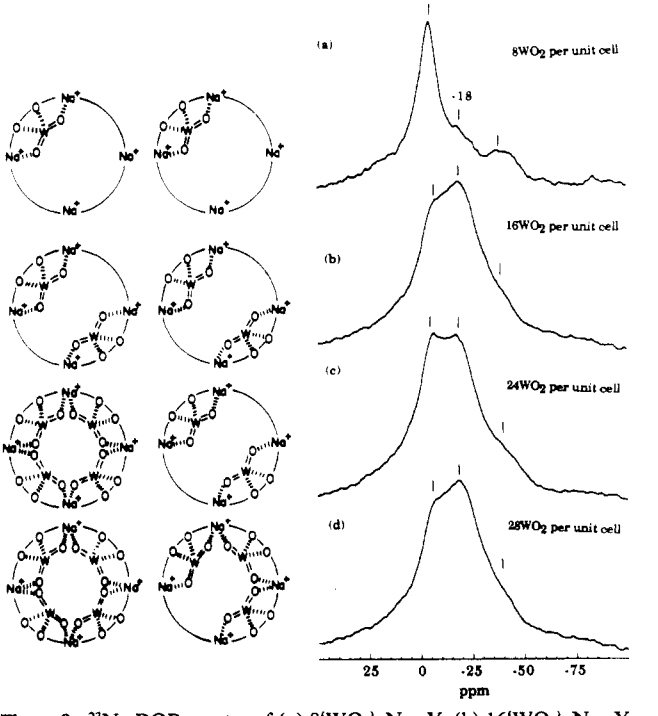

Figure 9. ^{23}Na DOR spectra of (a) $8\{WO_2\}$–$Na_{56}Y$, (b) $16\{WO_2\}$–$Na_{56}Y$, (c) $24\{WO_2\}$–$Na_{56}Y$, and (d) $28\{WO_2\}$–$Na_{56}Y$. A schematic illustration of the structural arrangement of the guest species in two adjacent α-cages is shown on the left on each spectrum.

ppm, of the prominent downfield resonance. This pronounced downfield shift from the original position of the site II signal from the precursor material at −23 ppm, Figure 6b, originates probably from the structural transformation undergone by the $W(CO)_6$ complexes inside the α-cage, as the formation of the W_2O_6 dimer might alter significantly the environment, and interaction strength, of the anchoring site II Na^+.

The first-stage thermal reduction product $16\{WO_{2.5}\}$–$Na_{56}Y$, reaction 2, consists of a supralattice of superexchange coupled (W^{5+}/W^{5+}) W_2O_5 dimers, whereas the final product,

16{WO_2}-$Na_{56}Y$, exists as separate WO_2 monomers, as illustrated in Figure 3.[11,12] Inspection of the DOR spectra in Figure 6 might support this structural picture. Hardly any difference is observed between the ^{23}Na spectra of the W_2O_6 and W_2O_5 loaded samples, Figure 6c,d, respectively. This is anticipated, since the basic dimer structure is retained in both materials. On the other hand, the thermally reduced sample, 16{WO_2}-$Na_{56}Y$, contains WO_2 monomers, each of which interacts with *two* Na^+ anchoring cations, twice as many as the dimeric species. Indeed, the ^{23}Na DOR spectrum of the final product, shown in Figure 6e, features a prominent signal at around −17 ppm which is ascribed to the anchoring Na^+ cations at site II. The anchoring Na^+ resonance is relatively broad, however, in particular compared to the respective site II Na^+ peak, at around −23 ppm, in the parent material 16{$W(CO)_6$}-$Na_{56}Y$, Figure 6b. This broadening might be brought about because of a relatively weak anchoring interaction between the oxygens of the oxotungsten bonds of WO_2 and the Na^+ cations, which allows a larger distribution of Na^+ environments (see discussion concerning the site II Na^+ signal in dehydrated $Na_{56}Y$, above). This interpretation is supported by spin–lattice relaxation measurements conducted in our laboratories[18] and might be related to a weaker Lewis basicity of the oxotungsten bond of WO_2, compared to the carbonyl group in the $W(CO)_6$ guest.

Figures 7–9 examine the loading effects of the various intrazeolite tungsten oxidation products as featured in the ^{23}Na DOR spectra. Since the maximum loading of the $W(CO)_6$ precursor is 16 molecules/per unit cell (two per α-cage), one uses a sequential saturation impregnation photooxidation (SIP) technique in order to achieve full-filling of the α-cages with WO_3 (and WO_2). The loading is represented by the reaction stoichiometries:

$$16\{M(CO)_6\}\text{-}Na_{56}Y \rightarrow 16\{MO_3\}\text{-}Na_{56}Y$$

$$8\{M(CO)_6\}\text{-}Na_{56}Y,\ 16\{MO_3\}\text{-}Na_{56}Y \rightarrow 24\{MO_3\}\text{-}Na_{56}Y$$

$$4\{M(CO)_6\}\text{-}Na_{56}Y,\ 24\{MO_3\}\text{-}Na_{56}Y \rightarrow 28\{MO_3\}\text{-}Na_{56}Y$$

$$\vdots$$

$$1\{M(CO)_6\}\text{-}Na_{56}Y,\ 31\{MO_3\}\text{-}Na_{56}Y \rightarrow 32\{MO_3\}\text{-}Na_{56}Y$$

Figure 7 shows the DOR spectra of a series of WO_3 loaded samples. An increase in the intensity of the shoulder at around −16 ppm, which corresponds to site II Na^+ cations, occurs upon increasing the loading from $8WO_3$/unit cell, Figure 7a, to $16WO_3$ per unit cell, Figure 7b. This increase is anticipated, as a larger number of Na^+ cations in the α-cage are anchored to the encapsulated W_2O_6 dimers in 16{WO_3}-$Na_{56}Y$. The DOR spectrum of 24{WO_3}-$Na_{56}Y$, Figure 7c, features a further increase in the total intensity assigned to the site II Na^+, accompanied by an upfield shift of the peak, to around −20 ppm. This shift might originate from the formation of the dimers-of-dimers structure upon loading more than a single W_2O_6 dimer in the α-cage, see schematic drawing, Figure 7c.

The ^{23}Na DOR spectra of the first-stage thermal reduction products, n\{$WO_{2.5}$\}-$Na_{56}Y$ (n = 8, 16, 24), are shown in Figure 8. The NMR results of the lower loading materials, $8WO_{2.5}$ and $16WO_{2.5}$ per unit cell, Figure 8a,b, respectively, exhibit a close similarity to the equivalent WO_3 loaded samples, Figure 7a,b, respectively. This resemblance underlines a similar structural arrangement of the two dimeric species, n\{WO_3\}-$Na_{56}Y$ and n\{$WO_{2.5}$\}-$Na_{56}Y$, when $n \leq 16$. The DOR result of the highest loading sample, 24{$WO_{2.5}$}-$Na_{56}Y$, shown in Figure 8c, is, however, markedly different from its WO_3-loaded counterpart, shown in Figure 7c. The spectrum features a broad peak at around −20 ppm, with a shoulder at around −5 ppm, which might correspond to the Gaussian peak, ascribed to Na^+ in site I. This profound spectral effect is probably related to the structural transformation undergone by the W_2O_5 dimers, upon increasing the loading beyond 16{$WO_{2.5}$}-$Na_{56}Y$. At that loading stage, two adjacent W_2O_5 dimers in an α-cage transform into a W_4O_{10} *tetramer*.[12]

The loading dependence results of the second-stage thermal reduction product, n\{WO_2\}-$Na_{56}Y$ (n = 8, 16, 24, 28) shown in Figure 9, are somewhat different from the WO_3 and $WO_{2.5}$ series. Each WO_2 monomer is anchored to *two* Na^+ cations located at site II, and therefore all the available Na^+ cations inside the α-cage will be already anchored at 16{WO_2}-$Na_{56}Y$, as illustrated schematically in Figure 3. Indeed, inspection of Figure 9b–d reveals almost no difference between the ^{23}Na DOR spectra of the samples loaded with 16 or more WO_2 monomers/unit cell. The intensity, as well as the shape, of the resonances ascribed to site II Na^+, at around −18 ppm, hardly change, as the sodium-anchoring arrangement in the three high-loading samples, n-\{WO_2\}-$Na_{56}Y$ (n = 16, 24, 28), is similar.

Conclusions

High-resolution ^{23}Na DOR provides an insight into site specific anchoring interactions in m\{$M(CO)_6$\}-$Na_{56}Y$ and n\{MO_{3-x}\}-$Na_{56}Y$, where M = Mo, W; $0 < m \leq 16$, $0 < n \leq 32$ and $0 \leq x \leq 1$. Analysis of the intensity, shape and position of the NMR resonances yields information on anchoring and structures of the guest species in the α-cage. Probing the environments of extraframework Na^+ cations, using the DOR technique, should enable one to investigate the chemical and physical properties of the zeolitic inner surfaces in unprecedented details.

Acknowledgment. This work was supported by the Director, Office of Energy Research, Office of Basic Energy Sciences, Materials and Chemical Sciences Division, U.S. Department of Energy under Contract No. DE-AC03-76SF00098. R.J. is grateful to Professor A. Pines for helpful conversations. G.A.O. acknowledges the Natural Science and Engineering Research Council (N.S.E.R.C.) of Canada's Operating and Strategic Grants Programmes for generous financial support.

Registry No. $Mo(CO)_6$, 13939-06-5; $W(CO)_6$, 14040-11-0.

References and Notes

(1) Breck, D. W. *Zeolite Molecular Sieves*, R.E. Kieger Publishing Company: Malabar, 1984.
(2) Ozin, G. A.; Stein, A.; Kuperman, A. *Angew. Chem., Adv. Mater.* **1989**, *101*, 373. Stucky, G. D.; MacDougall, J. *Science* **1990**, *247*, 669.
(3) Ozin, G. A.; Özkar, S. *J. Phys. Chem.* **1990**, *94*, 7556.
(4) Özkar, S.; Ozin, G. A.; Moller, K.; Bein, T. *J. Am. Chem. Soc.* **1990**, *112*, 9575.
(5) Thomas, J. M.; Vaughan, D. E. W. *J. Phys. Chem. Solids* **1989**, *50*, 449.
(6) Klinowski, J. *Prog. Nucl. Magn. Reson.* **1984**, *16*, 237.
(7) Fraissard, J.; Ito, T. *Zeolites* **1988**, *8*, 350.
(8) Wu, Y.; Chmelka, B. F.; Pines, A.; Davies, M. E.; Grobet, P. J.; Jacobs, P. A. *Nature* **1990**, *346*, 550. Jelinek, R.; Chmelka, B. F.; Wu, Y.; Grandinetti, P. J.; Pines, A.; Barrie, P. K.; Klinowski, J. *J. Am. Chem. Soc.* **1991**, *113*, 4097.
(9) Jelinek, R.; Özkar, S.; Ozin, G. A. *J. Am. Chem. Soc.*, in press.
(10) Wu, Y.; Sun, B. Q.; Pines, A.; Samoson, A.; Lippmaa, E. *J. Magn. Reson.* **1990**, *89*, 297.
(11) Ozin, G. A.; Malek, A.; Prokopowicz, R.; MacDonald, P. M.; Özkar, S.; Moller, K.; Bein, T. *Doping and Band-Gap Engineering of an Intrazeolite Tungsten(VI) Oxide Supralattice.* MRS Meeting, Anaheim, CA, 1991. Özkar, S.; Ozin, G. A.; Prokopowicz, R. *J. Am. Chem. Soc.*, submitted.
(12) Moller, K.; Bein, T.; Özkar, S.; Ozin, G. A. *J. Phys. Chem.* **1991**, *95*, 5276.
(13) Fitch, A. N.; Jobic, H.; Renouprez, A. *J. Phys. Chem.* **1986**, *90*, 1311.
(14) (a) Özkar, S.; Ozin, G. A. *Adv. Mater.* **1992**, *11*, 22. (b) Ozin, G. A.; Özkar, A; Macdonald, P. M. *J. Phys. Chem.* **1990**, *94*, 6939.
(15) Mortier, W. J.; Van den Bossche, E.; Uytterhoeven, J. B. *Zeolites* **1984**, *4*, 41.
(16) Jelinek, R.; Chmelka, B. F.; Stein, A.; Ozin, G. A. *J. Phys. Chem.*, in press.
(17) Prokopowicz, R.; Ozin, G. A.; Özkar, S. *J. Phys. Chem.*, in press.
(18) Jelinek, R.; Pines, A.; Özkar, S.; Ozin, G. A., manuscript in preparation.